Erosion behaviour of cold sprayed coatings made of CrMnFeCoNi high-entropy alloy or composite powders containing WC hard particles in a pure nickel matrix

Giacomo Cappelli, Shuo Yin, Rocco Lupoi
Trinity College Dublin, The University of Dublin, Department of Mechanical, Manufacturing & Biomedical Engineering, Dublin, Ireland

Abstract

The performance of two distinct coating materials under alumina particle impingement was tested in this study. CrMnFeCoNi and WC-Ni coatings were applied to 2205 duplex stainless steel substrates using cold spray method with nitrogen as the process gas. In between the substrate and the high entropy alloy coating, an interlayer coating of 316 stainless steel was used. The presence of WC particles in the WC-Ni composite coatings was confirmed by SEM cross sectional inspection. Following deposition, the coatings were heat treated in an air furnace. The influence of heat treatment holding time on the WC-Ni coatings was studied using chemical analysis by x-ray diffraction. Heat treatments peak temperatures for the WC/Ni-Ni and high entropy alloy coatings were 600°C and 550°C, respectively. Coatings microhardness and porosity volume fraction were measured for all the samples. The HEA coating outperformed the WC/Ni-Ni hardness but exhibited a higher level of porosity. The coatings were then subjected to erosion experiments using alumina particles with variable impact angles (30°, 60°, and 90°). To compare the different materials, an average erosion value was calculated for each target specimen. The WC/Ni-Ni as-sprayed coating was the most effective against a 60° impingement angle. The HEA coating, on the other hand, demonstrated greater resistance to impact angles of 30° and 90°. SEM was utilized to examine the eroded areas and determine the main mechanisms of erosion.

Introduction

Erosion problems are common in pneumatic and hydraulic systems due to the action of the processed mean. Sometimes this issue can be faced with design refinements changing the system at a base level. On the other hand, when design changes are not possible or not enough for preventing the problem, the selection of the proper material is of main focus. To further improve components toughness and wear resistance, hard material coatings are substantially applied using thermal spray methods such as laser cladding[1], plasma spray[2], high-velocity oxyfuel[3], and cold spray[4]. The most common coating material named as “cermets” consist of hard particles such as tungsten carbides or alumina oxides dispersed in a metal matrix usually made of cobalt or nickel.

Cold spray is an additive manufacturing process characterized by high deposition mass rate and low thermal stresses, while it can efficiently fabricate dense and thick metallic coatings[5]–[7]. However, the principle at the base of the particles adhesion to the substrate is related to particles plastic deformation. Therefore, this principle does not apply to hard and brittle particles, that are instead entrapped in the coating as a result of the ductile matrix action. Nowadays, a few researchers tried to deposit composite cermet coatings by cold spray with the goal of increasing the deposition efficiency and the quantity of ceramic particles embedded in the resulting coatings[8]. Some of them also tested the coating resistance under wear or impingement erosion of a slurry or dry particles[4].

Solid particle erosion (SPE), in particular, is a type of erosion that occurs when solid particles dragged by fluid media impact on a surface resulting in mass loss of the target. The use of cermet coatings in the protection of metallic materials from SPE has shown promising results[9], [10] as their resistance is generally superior to that of their metal matrix. Furthermore, the cermet hard particles-ductile matrix composition ratio is an important characteristic since the SPE mechanism is strongly dependent on the impingement angle. Indeed, it has been proven that ductile materials are considered to exhibit better erosion resistance at normal impingement angle, while brittle materials at lower angles (60°, 30°) [7,15]. In addition to the impingement angle the SPE behaviour is also influenced by the erodent properties such as feed rate, velocity, size, and hardness. In the present study, we were interested in comparing the erosion resistance of CrMnFeCoNi and WC-Ni coatings. During this study, an attempt was made to raise the concentration of WC in the coating, but no positive results were obtained.

As previously discussed, in the past years, wear and erosion problems have been mainly faced with the application of hard ceramic materials embedded in a metal matrix. In this study, the erosion behaviour of a cold sprayed high entropy alloy (HEA), in particular the Cantor CrMnFeCoNi was tested. Even though HEA are becoming popular in the scientific community, the behaviour against impingement erosion of this particular alloy has not been assessed yet, being part of the novelty provided by this study.

HEAs are not easily deposited through cold spray since they require helium as process gas or really high working parameters for cold spray systems employing nitrogen[11]–[14]. However, deposition of this material through cold spray may lead to hardness improvements due to the combination of HEAs high work hardening behaviour and the particles plastic deformation induced by the process. To boost coating adhesion, a stainless-steel interlayer was previously placed and adopted between the substrate and the HEA coating.

Experimental procedure

Powders and substrate

The feedstock powders used in this study were produced by blending the composite powder WC/Ni (Amperit 547.074, – 45 + 15 µm) from Hoganas and pure Ni powder (– 45 + 16 µm) from Praxair. The powders were mixed at three different

concentrations: 70%, 80% and 90% of WC/Ni volume fraction with the pure Ni powder as balance. The used HEA powder was CrMnFeCoNi (– 45 + 10 µm) provided by H.C.Starck. The coated substrates were as-machined 4 mm thick 2205 duplex stainless steel (1.4462) plates and cleaned with ethanol. Stainless steel 316 powder from Carpenter Additive was also adopted for the realization of an interlayer between the substrate and the HEA coatings.

Cold spray deposition and heat treatments

For the coatings manufacturing, a custom-made cold spray system (Trinity College Dublin, Ireland) was used. The system is equipped with a powder feeder PF100WL from Uniquecoat Technologies LLC used at a powder feed rate of 80 g/min. For any feedstock material nitrogen was used as process gas, and the gas temperature and pressure were set at the highest achievable values of 900°C and 30 bar, respectively. The particles were accelerated through a WC–Co De Laval nozzle with a divergent length of 190 mm, throat diameter of 3 mm, and outlet diameter of 8 mm. The nozzle–substrate spray distance was set at 40 mm while the nozzle travel speed at 50 mm/s. For each one of the tested feedstocks, three layers were deposited following a zig-zag pattern with 1 mm of step distance between parallel lines. In the case of HEA coatings, an interlayer of about 700 µm thickness was deposited in SS316 to facilitate the adhesion of the consequent sprayed Cantor alloy powder.

After fabrication, the WC-Ni coatings were heat treated at 600°C with a heating ramp rate of 10°C/min. Dwell times of 1 h, 2 h and 3 h were performed to see if there are any microstructural changes depending on the duration. Slow cooling was performed in the furnace. Some of the SS316 interlayers were annealed before HEA deposition at 1000°C for 4 h dwell time. After HEA deposition, specimens were heat treated at 550°C for 1 h. All the heat treatments were performed in a Carbolite RHF1600 air furnace.

Material characterization

Powders and specimens were analysed at the Scanning Electron Microscope (SEM, Carl Zeiss ULTRA, CRANN). The SEM parameters were set at 5 kV of accelerating voltage and 8.5 mm of working distance. Samples cross sections were extracted using wire EDM (Excetex V440G) and then prepared using 320, 600, 1200, 2500 grinding papers and 6 to 1 micron suspended solution on polishing clothes. Colloidal silica suspension was also used as last polishing step. Microhardness measurements were performed on the polished cross-sections averaging the results of fifteen indentations conducted with a Vickers tester (ZwickRoell ZHV30). For the measurements a load of 500gf was applied for 10 seconds. Coating porosity was estimated using ImageJ software with images collected at the SEM at x250 magnification. The Trainable Weka Segmentation plugin of ImageJ was used to estimate the amount of WC particles entrapped in the deposited coatings. To evaluate the influence of heat treatments on the chemical composition of WC-Ni coatings, an X-ray-diffraction system (TBSI, Trinity College) was used. Coatings density was measured by Archimedes method using a scale apparatus equipped with a density determination kit (Ohaus Explorer). By Archimedes principle [15], the volume of the sample (V_s) and the density (ρ_s) can be expressed as:

Equation 1

$$V_s = \frac{m_s - m_{sf}}{\rho_y}$$

Equation 2

$$\rho_s = \frac{m_s}{V_s} = \frac{m_s}{m_s - m_{sf}}\rho_y$$

Where ρ_y is the liquid density and m_s and m_{sf} are the sample dry and submerged mass, respectively.

Solid particle erosion tests

Solid particle erosion tests (SPE) were conducted using angular shaped alumina erodent particles with 50 µm average size (Figure 1) carried by compressed air at the pressure of 1.5 bar. A scheme of the used apparatus is shown in Figure 3: Solid particle erosion test apparatus.. The used nozzle has a length of 105 mm with a constant internal diameter of 3 mm. The tests were performed at room temperature and lasted 10 min for each specimen. The specimens were 30 mm diameter coated disks. Before the erosion test, the coatings were prepared by machining until 1 mm of coating thickness was reached. Then, the specimens' surface was grinded with 320 paper and cleaned with ethanol. The SPE were conducted at 90°, 60° and 30° impacting angles and the distance between the nozzle and the target was set to 10 mm. Any test combination was repeated two times to get a more reliable estimate of the erosion behaviour. Each specimen was weighed before and after the erosion test using a 4 decimal weighing scale (Ohaus Discovery) to record the mass loss. Process time and erodent particles feed rate were recorded throughout all the tests. To compare the results of the different materials, an average erosion value ($mm^3\backslash g$) was used. The average erosion value was calculated by dividing the erosion rate (mg/s) by the abrasive flow rate (g/s) and then dividing again by the specimen density (g/cm^3) measured by Archimedes. The erosion test was conducted following the ASTM G76-18 standard[16].

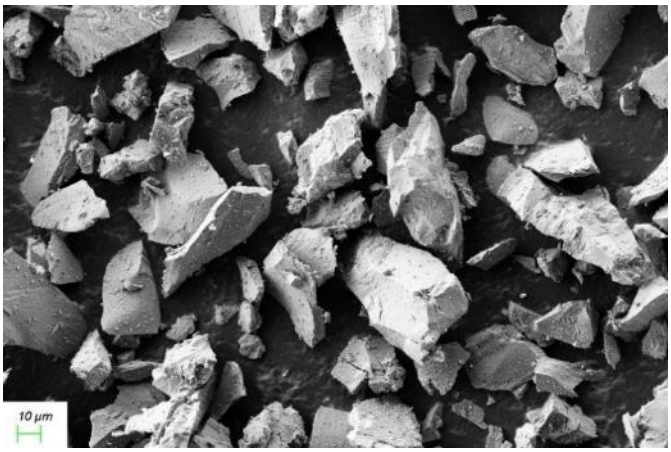

Figure 1: Alumina erodent particles.

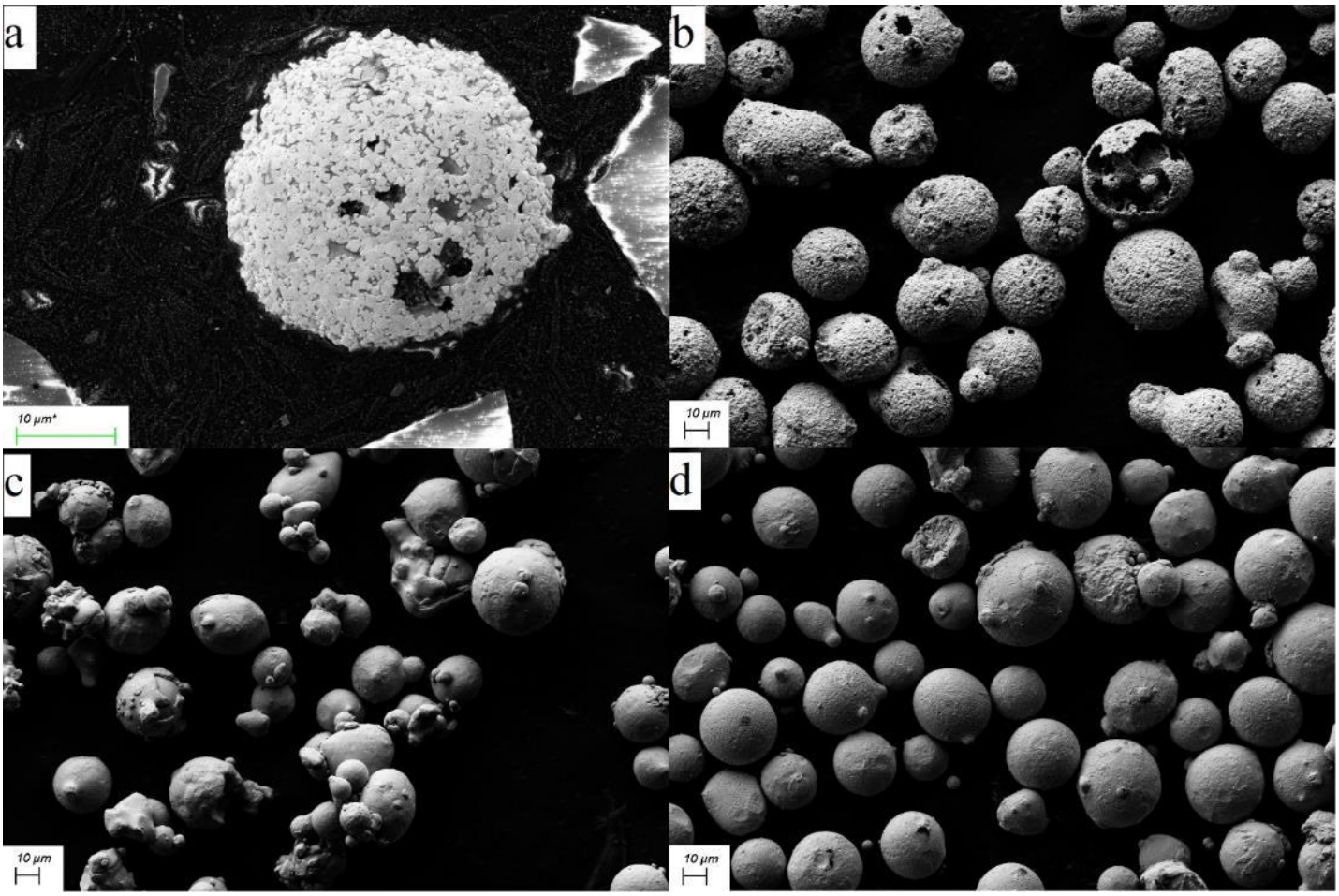

Figure 2: Electron micrographs of the feedstock powders, a) composite WC/Ni powder cross section, b) composite WC/Ni powder, c) Nickel powder, d) CrMnFeCoNi powder.

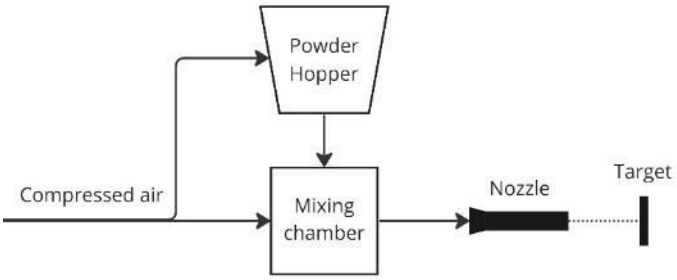

Figure 3: Solid particle erosion test apparatus.

Results and discussions

Powder characterization

Images collected at the scanning electron microscope of the used feedstock powders are shown in Figure 2. The WC/Ni composite powder is depicted in Figure 2a-b. This powder consists of nanosized tungsten carbide particles agglomerated in a nickel porous matrix that facilitate the powder deposition. The feedstock powder for the WC-Ni coatings was made by mixing the WC/Ni composite powder with the pure nickel powder displayed in Figure 3c. The latter is instead characterised by the typical compact and spherical morphology as in the case of the CrMnFeCoNi HEA powder shown in Figure 2d.

Coatings characterization

First of all, this study was focused on testing different WC/Ni-Ni feedstock powder compositions, increasing the concentration of WC/Ni composite powder in the feedstock from 70% of volume fraction to 90%, in line with what was done by Alidokht et al.[17] where they achieved a maximum of 54% volume concentration of WC entrapped in the coating. In the present study, deposition was obtained only when spraying the feedstock powder containing 70% volume fraction of WC/Ni powder, whereas with the 80 vol% and 90 vol% of WC/Ni concentration feedstock no deposition was obtained. A cross section of the obtained coating is shown in Figure 4a. WC particles, in light grey, are easily distinguishable with respect to the nickel matrix, darker grey areas. The average WC concentration was estimated to be 42.5±8 vol% by image analysis. In Figure 4a, small cracks are visible in the nickel matrix (red arrows), which were most likely caused by the impacting WC particles' severe compaction effect on the nickel matrix. Cracks, on the other hand, were no longer detectable in the specimens subjected to heat treatment (Figure 4b).

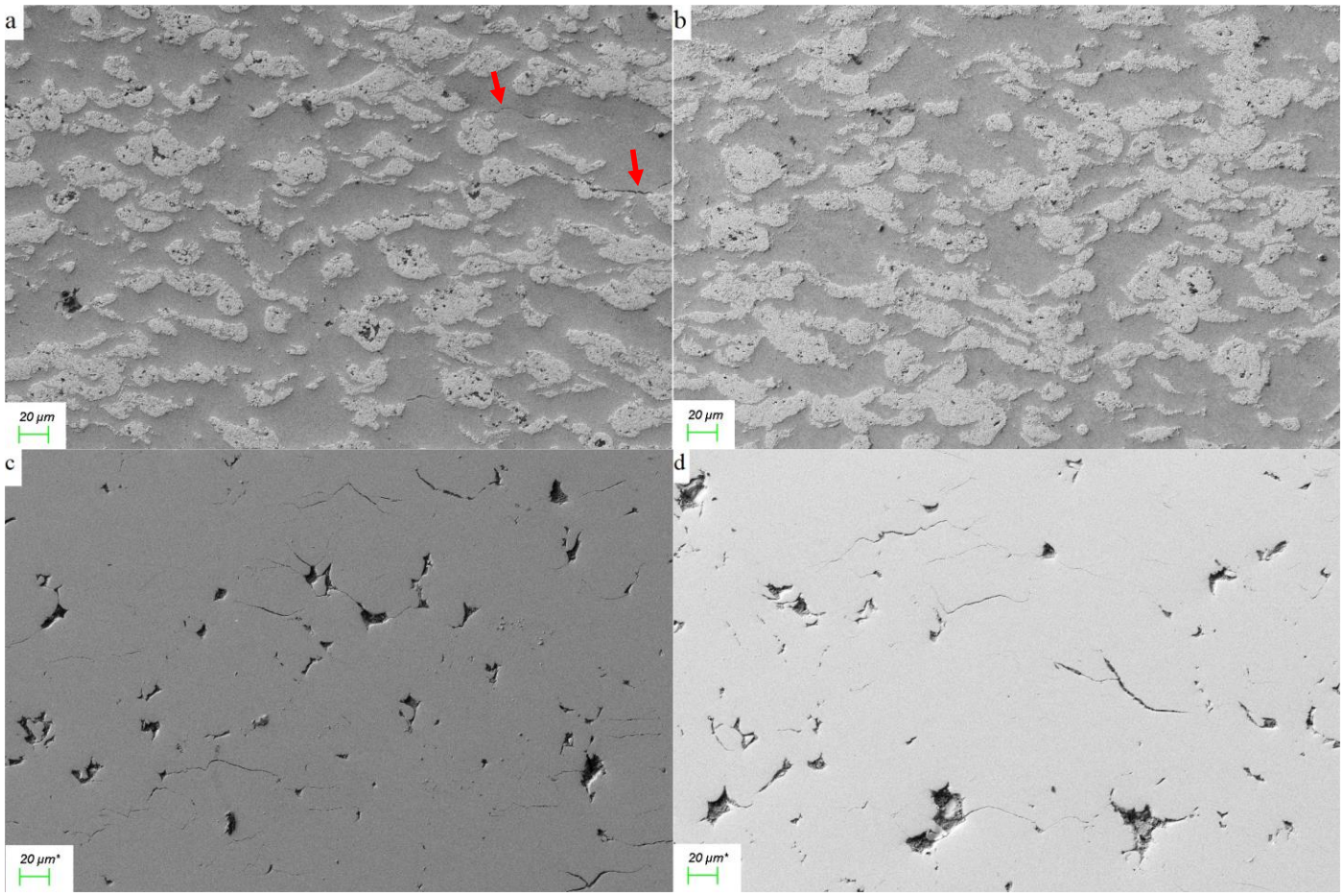

Figure 4: Electron micrographs at x250 magnification of cold sprayed coatings. a) WC/Ni-Ni coating in as sprayed condition, b) WC/Ni-Ni coating after heat treatment at 600°C for 1 hour in air, c) As sprayed CrMnFeCoNi HEA coating, d) CrMnFeCoNi HEA coating after heat treatment at 550°C for 2 hours in air.

Results of the chemical analysis by x-ray diffraction are displayed in Figure 5. The chemical analysis was performed on three samples of WC/Ni-Ni coatings that were subjected at different heat treatments. All of them were heat treated at the temperature of 600°C in a Carbolite air furnace, but holding time was tested at 1 hour, 2 hours and 3 hours. As a result, the XRD analysis was performed to determine whether varying holding times resulted in different phase changes. As can be seen in the XRD plot of Figure 5, nickel is the main component with WC, but many oxides of both nickel and tungsten were formed during the heat treatment in air. Furthermore, as can also be expected, the concentration of oxides seems to increase with the holding time. Therefore, after chemical analysis by X-ray diffraction, the selected heat treatment holding time for the WC/Ni-Ni coatings to be used for erosion testing was of 1 hour. However, no decarburization of tungsten was recorded in any of the specimens, preventing that phenomenon to be related to the holding time. Besides, the annealing heat treatment resulted to be effective in reducing the coatings porosity. Indeed, in the as-sprayed condition, the porosity was found to be 1.4±0.5 vol%, whereas in the heat-treated condition the porosity decreased to 0.7±0.2 vol%. The reduction in porosity that occurred may be related to the aforementioned crack closure and subsequent densification of the coating.

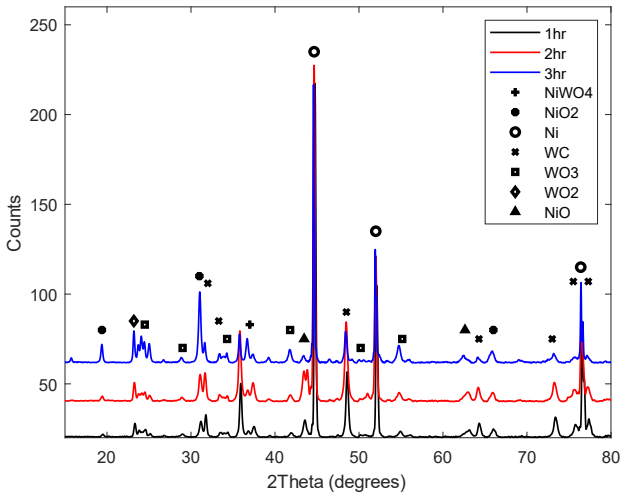

Figure 5: X-ray diffraction results of the WC/Ni-Ni coatings after heat treatment in air at 600°C varying the dwell time.

The coating microhardness in the as sprayed and heat-treated conditions were estimated as 370±58 and 252±39 HV0.5, respectively. The drop in microhardness after heat treatment is in line with what was recorded by Kazasidis et al. [18]. They attributed the cause of this drop to the nickel recrystallization that normally occurs at temperatures between 370 to 700 °C.

Table 1: Solid particle erosion tests results of WC/Ni-Ni coating in the as sprayed and heat-treated conditions.

	AS WC/Ni-Ni						HT WC/Ni-Ni					
Angle	90°		60°		30°		90°		60°		30°	
Mass loss [mg]	42	46	49	45	74	60	58	52	70	71	55	72
Erodent feed rate [g/s]	0.041	0.031	0.048	0.037	0.035	0.028	0.035	0.027	0.036	0.032	0.032	0.029

Furthermore, the work hardening undergone by the particles during deposition might have further reduced the recrystallization temperature.

Spray tests with CrMnFeCoNi HEA powder on duplex 2205 stainless steel substrates were characterized by coating delamination that occurred periodically throughout the deposition process. Symptoms of the two materials' incompatibility. Therefore, the choice of substrate material was blamed for the unsatisfactory results. As a result, an interlayer coating made of 316 stainless steel was used to enable the HEA coating built up. The deposited stainless-steel layer was 700 µm thick on average and was employed at the as-sprayed surface condition since the substrate roughness may promote future HEA layer adherence. However, half of the specimens were heat treated at 1000°C for 4 hours in air furnace ([19], [20]) since the softening of the 316 stainless steel interlayer might further improve the CrMnFeCoNi coating adhesion. HEA deposition was then successfully obtained on the SS316 interlayers. Subsequently, the specimens were subjected to heat treatment at 550°C for 2 hours in air furnace to release residual stresses and reduce the coating porosity. The porosity of the HEA coatings deposited on SS316, and heat-treated SS316 (HTSS316) was 1.8±0.4 vol% and 1.1±0.2 vol%, respectively. The average microhardness was 420±41 HV0.5 for the HEA deposited on SS316 and 430±50 HV0.5 for HEA coating on HTSS316 interlayer. The microhardness results were consistent with the ones obtained by Ahn et al. [12] who conducted an heat treatment with the same temperature and holding time in argon atmosphere. They recorded a 0.3 vol% of porosity in their coatings, that was achieved using helium as process gas. In contrast, in this study even after heat treatment, significant porosity was still present in the coatings, as can also be seen in Figure 4c-d. In the figure, microcracks, pores, and inter-particle boundaries are evident, indicating that the metallic bonding is incomplete. However, a significant reduction in porosity resulted between HEA deposition on as sprayed and heat treated SS316, illustrating the beneficial impact of the interlayer's annealed state prior to HEA deposition.

The microhardness of all the deposited coatings in this study are compared in Figure 6. Despite the entrapped hard WC particles, the microhardness of the HEA coatings outperformed the composite WC-Ni coatings. That is because the overall hardness of the WC/Ni-Ni coating is the result of an average between the ductile nickel matrix and the dispersed hard particles. The diagram also shows the significant reduction in hardness of the WC/Ni-Ni coating following annealing heat treatment.

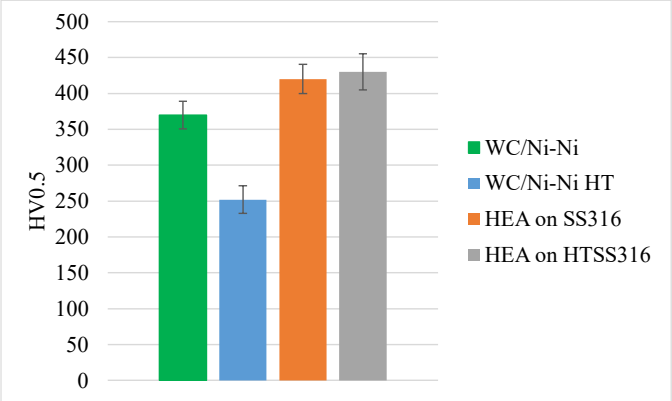

Figure 6: Microhardness HV0.5 comparison among coatings made of WC/Ni-Ni, WC/Ni-Ni after heat treatment, heat treated HEA on SS316 and heat-treated HEA on HTSS316.

Erosion behaviour

Following the erosion test, any sample was weighed, and the mass loss due to impact erosion was determined by subtracting the post-erosion specimen mass from the pre-erosion specimen mass. In Table 1 and Table 2 the computed mass losses for any specimen under the different impacting angles are listed. Paired with the mass losses, the recorded erodent feed rates for any test are indicated. Any material-impact angle test combination was repeated two times. The majority of the coupled tests were consistent with each other since the resulting mass losses of the two repetitions were really similar. Anyway, small deviations in the mass loss were expected because of the slightly variation in the erodent feed rate throughout the experimental campaign. To make the results independent from the erodent feed rate an average erosion value that expresses the volume of the removed material per grams of sprayed erodent was computed. To do that, the coatings density was computed through Archimedes principle using Equation 2 and coating parts collected from the specimens. The estimated densities were 10.059 g/cc and 7.817 g/cc for the WC/Ni-Ni and HEA coatings, respectively. Therefore, the average erosion rate was calculated by dividing the erosion rate (mg/s) by the abrasive flow rate (g/s) and then dividing by the specimen density (g/cm^3) measured by Archimedes. The obtained results are plotted in Figure 7.

Coating erosion appears to increase when the impact angle decreases in all of the tested materials. However, the mass loss among the several test settings is less variable in the heat-treated WC/Ni-Ni coating than in the as-sprayed condition, showing a lower difference in erosion resistance among tests performed at 90°, 60° and 30° impact angles. The mass loss in the as-sprayed condition, on the other hand, is quite similar in the 90° and 60°

Table 2: Solid particle erosion tests results of HEA coatings on as sprayed and heat treated SS316 conditions.

	HEA on SS316						HEA on HTSS316					
Angle	90°		60°		30°		90°		60°		30°	
Mass loss [mg]	32	32	41	42	61	62	31	29	43	42	61	62
Erodent feed rate [g/s]	0.058	0.032	0.032	0.034	0.039	0.052	0.027	0.029	0.033	0.039	0.045	0.027

tests and significantly increases when the impact angle is set to 30°. In this case, what obscures the relationship between mass loss and impact angle could be the change in concentration of dispersed WC particles in the impact area.

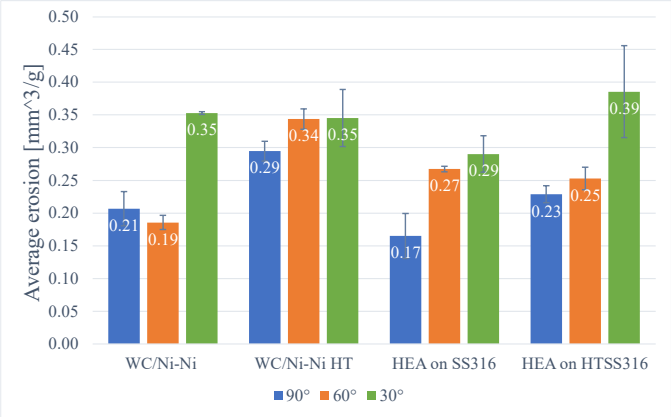

Figure 7: Average erosion results of the solid particle erosion tests conducted on WC/Ni-Ni as sprayed and heat-treated coatings, and HEA coatings on as sprayed and heat treated SS316.

When considering HEA coatings, the mass loss dependency on the impact angle is evident, as the mass loss grows in the same way in both material states and can be easily described by a second-degree polynomial function that rapidly increases when the angle approaches zero.

Considering the average erosion values of Figure 7, some of the aspects highlighted by the mass losses are confirmed. The heat-treated WC/Ni-Ni coating for instance shows the least variable behaviour at changes of the impact angle. Besides, erosion of the HEA coatings clearly becomes stronger as impact angle decreases. An interesting result is instead the one of the as-sprayed WC/Ni-Ni coating under 60° angle, since the average erosion is even slightly lower than the one recorded at 90° impact angle. Despite having approximately equal average hardness, HEA deposited on SS316 demonstrated to be more resistant to particle impact erosion at 30° impact angle than the same material applied on the annealed stainless-steel interlayer. Furthermore, the HEA coating deposited on SS316 showed to undergo a lower erosion under normal impact angles with respect to the HEA coating deposited on HTSS316. In this case the higher level of porosity volume fraction characterizing the HEA on SS316 coating may be the cause, since the impacting particles perform a compacting action on the coating, that deforms closing the gaps instead of losing material.

From the obtained results we can conclude that the HEA coating deposited on the as-sprayed 316 stainless steel is the one showing the highest resistance against the most critical condition, that is at 30 degrees of impact angle. Furthermore, the same coating stands out when subjected to erodent particles impact at normal angle. However, at intermediate angles (60°),

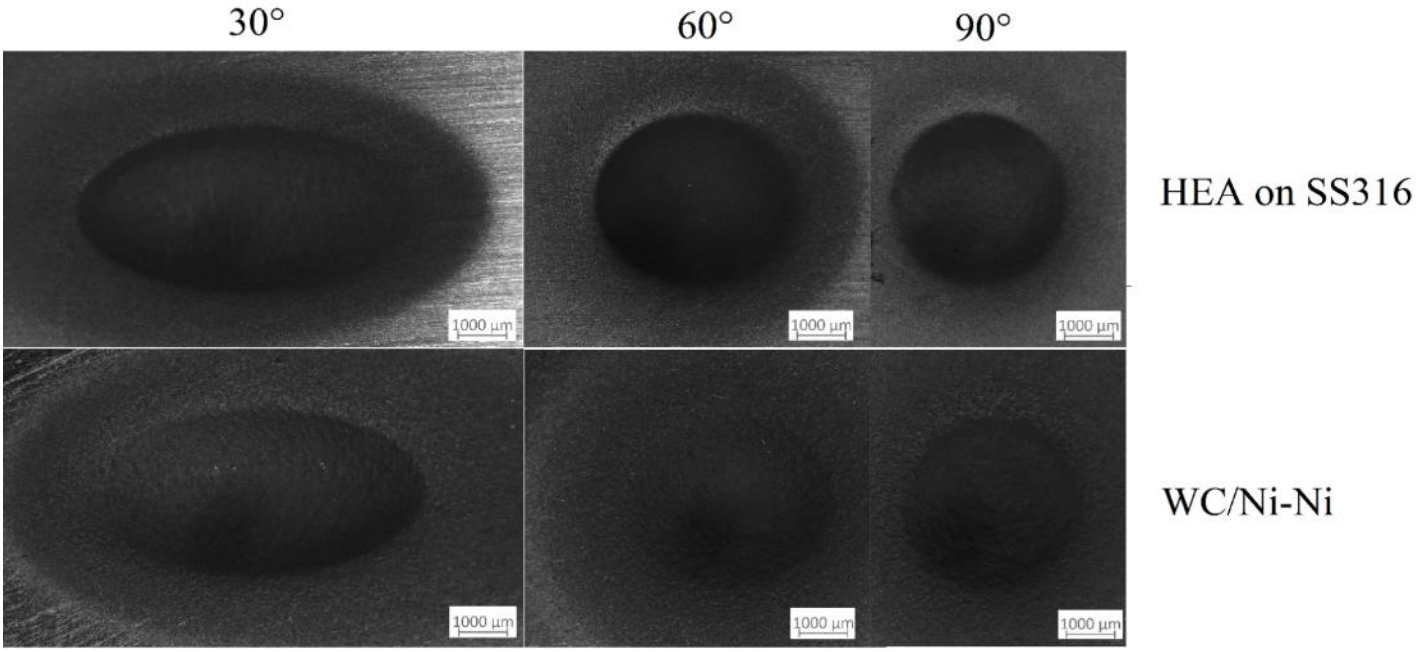

Figure 8: Imprints after solid particle erosion tests on the HEA coating on as-sprayed 316 stainless-steel interlayer and WC/Ni-Ni as-sprayed coating.

the WC/Ni-Ni at the as-sprayed condition was the most resistant among the tested materials.

The imprints left in any of the samples did not achieve 1 mm of depth, so the erosion process was limited to the coating and did not reach the substrate material. On average the imprints were 500 µm deep, so in line with the erosion limit imposed by the ASTME G76 – 18 standard. The imprints made on the HEA and WC/Ni-Ni coatings are displayed in Figure 8: Imprints after solid particle erosion tests on the HEA coating on as-sprayed 316 stainless-steel interlayer and WC/Ni-Ni as-sprayed coating. All the imprints are featured by a central deep zone and a round shape that is circular under 90 degrees impact angles and becomes elliptical as the angle is reduced.

Electron micrographs of the eroded areas of the heat-treated WC/Ni-Ni coating and of the Cantor alloy coating on the heat treated SS316 interlayer are shown in Figure 9. As expected for the WC/Ni-Ni coatings, the action of the erodent particles impacting at 30° affects mainly the nickel matrix by ploughing and not the tungsten carbides (Figure 9a). At low impact angles indeed, the particles slide and abrades the surface, but the coating behaviour changes depending on the local concentration of WC. The eroded area results therefore to have an irregular morphology, since the nickel matrix undergoes a significant erosion, while the WC rich areas show a higher strength resulting in an eroded surface characterized by cavities and protrusions. Increasing the impact angle the erosion mechanism changes resulting in striations, craters, and pits formation (Figure 9b-c). Cracked erodent alumina particles appear to be retained in the coating as the impact angle approaches 90°. On the other hand, at a 30° angle, the alumina particles are more likely to rebound after impinging and not consolidate in the coating.

In the Cantor HEA coating, the eroded surface is more regular with respect to the WC/Ni-Ni coatings, since in this case the material properties are more homogeneous. Under 30° impact angles the main mechanism is still ploughing with addition of striations and pits (Figure 9d). At 60° and 90° angles the ploughing effect is less substantial, and craters, cavities and cracks formation become more probable under the impact of the erodent particles (Figure 9e-f).

Conclusions

The microstructure and erosion resistance to alumina particle impingement of a tungsten carbide and nickel composite coating and a CrMnFeCoNi high entropy alloy coating were investigated. From the study, the following conclusions can be drawn:

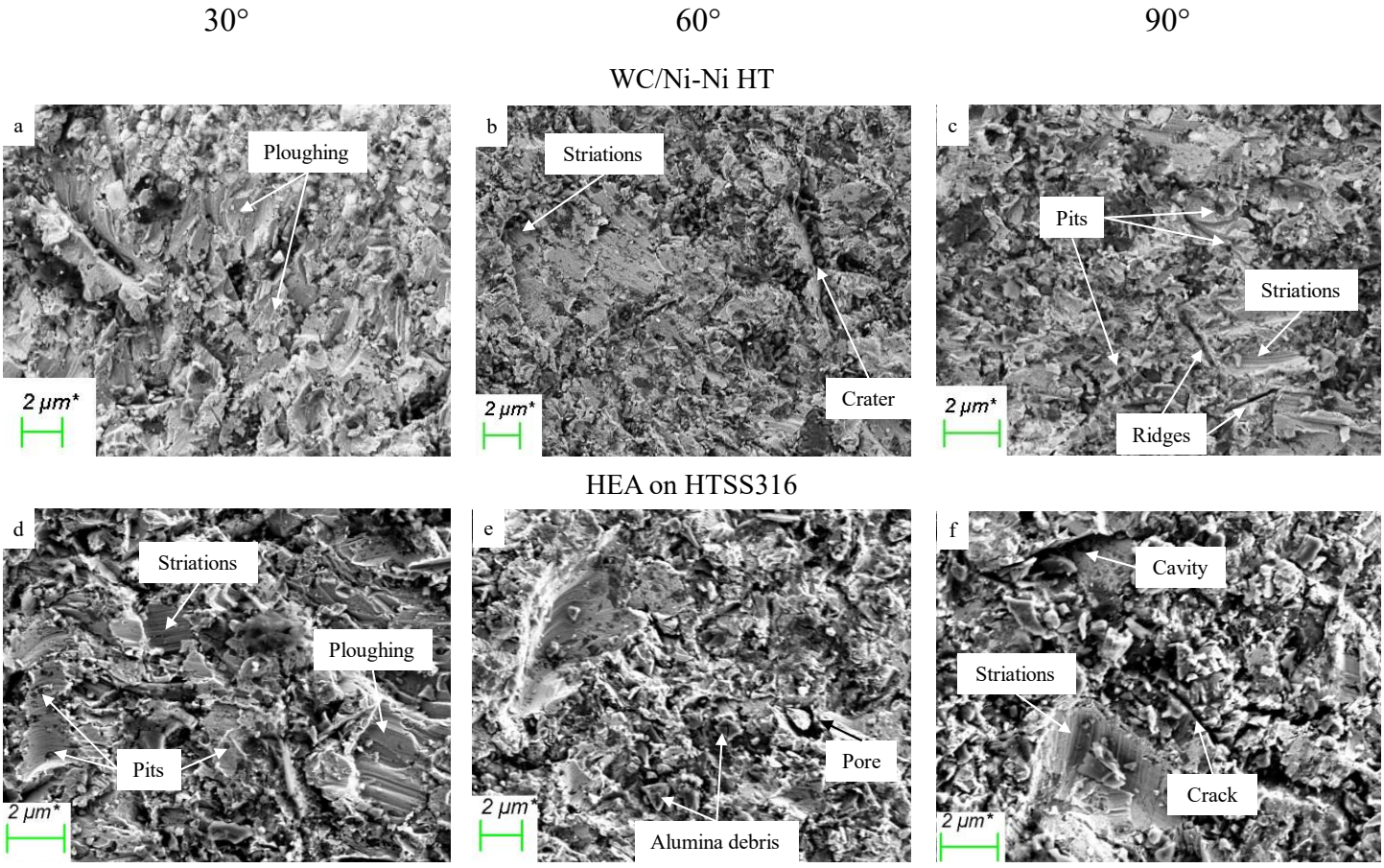

Figure 9:electron micrographs of the eroded areas. a) WC/Ni-Ni HT coating at 30° impact, b) WC/Ni-Ni HT coating at 60° impact, c) WC/Ni-Ni HT coating at 90° impact, d) HEA on HTSS316 coating at 30° impact, e) HEA on HTSS316 coating at 60° impact, f) HEA on HTSS316 coating at 90° impact.

- WC/Ni-Ni composite coating was successfully deposited on 2205 duplex stainless steel estimating a 43 vol% of entrapped WC particles.
- CrMnFeCoNi high entropy alloy was successfully deposited on a 316 stainless steel coating interlayer deposited on a 2205 duplex stainless steel substrate.
- After 1 hour of heat treatment at 600°C in air, the porosity of the WC/Ni-Ni coatings decreased from 1.4 vol% to 0.7 vol%, and the microhardness decreased from 370±58 to 252±39 HV0.5.
- After heat treatment, the porosity of the HEA coatings deposited on SS316, and heat-treated SS316 (HTSS316) was 1.8±0.4 vol% and 1.1±0.2 vol%, respectively. The average microhardness HV0.5 were 420±41 for the HEA on SS316 and 430±50 for the HEA on HTSS316.
- In general, as the impact angle was lowered, the mass loss of all samples increased, with the 30° condition proving to be the most critical of the experimental campaign.
- After heat treatment, the WC/Ni-Ni coating's erosion behaviour became less susceptible to variations in impact angle.
- At 60° impact angle, the as-sprayed WC/Ni-Ni coating exhibited the lowest erosion.
- The HEA on SS316 coating appears to have the highest strength against alumina particles impinging at 90° and 30° impact angles among the tested coating materials.

Acknowledgments

The authors would like to express their gratitude to SchuF Valve Technology GmbH and ESA for their financial assistance (4000137618/22/NL/GLC/idb). The authors would like to also thank Trinity College Dublin's CRANN Advanced Microscopy Laboratory (AML) for its assistance in the microscopy characterisation and analysis.

References

[1] C. P. Paul, S. K. Mishra, P. Tiwari, and L. M. Kukreja, "Solid-Particle Erosion Behaviour of WC/Ni Composite Clad layers with Different Contents of WC Particles," *Opt. Laser Technol.*, vol. 50, pp. 155–162, 2013, doi: 10.1016/j.optlastec.2013.03.002.

[2] J. R. T. Branco, R. Gansert, S. Sampath, C. C. Berndt, and H. Herman, "Solid particle erosion of plasma sprayed ceramic coatings," *Mater. Res.*, vol. 7, no. 1, pp. 147–153, 2004, doi: 10.1590/s1516-14392004000100020.

[3] Y. Lian and Y. Li, "Investigation on erosion resistance of WC-Co-Cr coatings," *Tribol. Online*, vol. 13, no. 2, pp. 36–42, 2018, doi: 10.2474/trol.13.36.

[4] M. Kazasidis, E. Verna, S. Yin, and R. Lupoi, "The effect of heat treatment and impact angle on the erosion behavior of nickel-tungsten carbide cold spray coating using response surface methodology," *Emergent Mater.*, vol. 4, no. 6, pp. 1605–1618, 2021, doi: 10.1007/s42247-021-00274-7.

[5] V. K. Champagne, *The cold spray materials deposition process: Fundamentals and applications*. 2007.

[6] R. T. Sataloff, M. M. Johns, and K. M. Kost, *Modern Cold Spray*. Springer, 2015.

[7] G. Motors, S. N. Laborato-, and F. M. Company, *Cold spray technology*. .

[8] S. A. Alidokht and R. R. Chromik, "Sliding wear behavior of cold-sprayed Ni-WC composite coatings: Influence OF WC content," *Wear*, vol. 477, no. November 2020, p. 203792, 2021, doi: 10.1016/j.wear.2021.203792.

[9] S. Yin, E. J. Ekoi, T. L. Lupton, D. P. Dowling, and R. Lupoi, "Cold spraying of WC-Co-Ni coatings using porous WC-17Co powders: Formation mechanism, microstructure characterization and tribological performance," *Mater. Des.*, vol. 126, no. April, pp. 305–313, 2017, doi: 10.1016/j.matdes.2017.04.040.

[10] R. G. Rateick, K. R. Karasek, A. J. Cunningham, K. C. Goretta, and J. L. Routbort, "Solid-particle erosion of tungsten carbide/cobalt cermet and hardened 440C stainless steel-A comparison," *Wear*, vol. 261, no. 7–8, pp. 773–778, 2006, doi: 10.1016/j.wear.2006.01.012.

[11] C. J. Akisin, C. J. Bennett, F. Venturi, H. Assadi, and T. Hussain, "Numerical and Experimental Analysis of the Deformation Behavior of CoCrFeNiMn High Entropy Alloy Particles onto Various Substrates During Cold Spraying," *J. Therm. Spray Technol.*, vol. 31, no. 4, pp. 1085–1111, 2022, doi: 10.1007/s11666-022-01377-1.

[12] J. E. Ahn, Y. K. Kim, S. H. Yoon, and K. A. Lee, "Tuning the Microstructure and Mechanical Properties of Cold Sprayed Equiatomic CoCrFeMnNi High-Entropy Alloy Coating Layer," *Met. Mater. Int.*, vol. 27, no. 7, pp. 2406–2415, 2021, doi: 10.1007/s12540-020-00886-4.

[13] J. Mahaffey, A. Vackel, S. Whetten, M. Melia, and A. B. Kustas, "Structure Evolution and Corrosion Performance of CoCrFeMnNi High Entropy Alloy Coatings Produced Via Plasma Spray and Cold Spray," *J. Therm. Spray Technol.*, vol. 31, no. 4, pp. 1143–1154, 2022, doi: 10.1007/s11666-022-01373-5.

[14] R. Nikbakht *et al.*, "Cold Spray and Laser-Assisted Cold Spray of CrMnCoFeNi High Entropy Alloy Using Nitrogen as the Propelling Gas," *J. Therm. Spray Technol.*, vol. 31, no. 4, pp. 1129–1142, 2022, doi: 10.1007/s11666-022-01361-9.

[15] C. Wei, Z. Liu, Y. Bao, D. Wan, Y. Qiu, and X. Liu, "Evaluating thermal expansion coefficient and density of ceramic coatings by relative method," *Mater. Lett.*, vol. 161, pp. 542–544, 2015, doi: 10.1016/j.matlet.2015.09.034.

[16] Astm, "G76-07, Standard Test Method for Conducting Erosion Tests by Solid Particle Impingement Using Gas Jets," *ASTM Int.*, vol. i, pp. 1–6, 2013, doi: 10.1520/G0076-18.2.

[17] S. A. Alidokht, P. Vo, S. Yue, and R. R. Chromik, "Cold Spray Deposition of Ni and WC-Reinforced Ni Matrix Composite Coatings," *J. Therm. Spray Technol.*, vol. 26, no. 8, pp. 1908–1921, 2017, doi: 10.1007/s11666-017-0636-4.

[18] M. Kazasidis, E. Verna, S. Yin, and R. Lupoi, "Investigation of the Effect of Low-Temperature Annealing and Impact Angle on the Erosion Performance of Nickel-Tungsten Carbide Cold Spray Coating Using Design of Experiments," *Therm. Spray 2022 Proc. from Int. Therm. Spray Conf.*, vol. 84369, pp. 763–772, 2022, doi: 10.31399/asm.cp.itsc2022p0763.

[19] S. Yin, J. Cizek, X. Yan, and R. Lupoi, "Annealing strategies for enhancing mechanical properties of additively manufactured 316L stainless steel deposited by cold spray," *Surf. Coatings Technol.*, vol. 370, no. April, pp. 353–361, 2019, doi: 10.1016/j.surfcoat.2019.04.012.

[20] S. Bagherifard *et al.*, "Tailoring cold spray additive manufacturing of steel 316 L for static and cyclic load-bearing applications," *Mater. Des.*, vol. 203, p. 109575, 2021, doi: 10.1016/j.matdes.2021.109575.